PCCP

RSC Publishing

PAPER

View Article Online
View Journal | View Issue

High-resolution anion photoelectron spectra of TiO_2^-, ZrO_2^-, and HfO_2^- obtained by slow electron velocity-map imaging

Cite this: *Phys. Chem. Chem. Phys.*, 2013, **15**, 20973

Jongjin B. Kim,[a] Marissa L. Weichman[a] and Daniel M. Neumark*[ab]

Received 26th September 2013,
Accepted 22nd October 2013

DOI: 10.1039/c3cp54084g

www.rsc.org/pccp

High-resolution anion photoelectron spectra of the Group 4 metal dioxides TiO_2^-, ZrO_2^-, and HfO_2^- are reported, using slow electron velocity-map imaging (SEVI) combined with ion trapping and cryogenic cooling. The resulting spectra exhibit sub-meV resolution with no congestion from hot bands. Electron affinities are obtained with greater precision than in previous photodetachment experiments, with values of 1.5892(5) eV, 1.6397(5) eV, and 2.1045(5) eV, for TiO_2, ZrO_2, and HfO_2, respectively. We obtain precise values for all of the vibrational frequencies of the neutral $\tilde{X}^1A_1$ ground states, except for the ν_3 mode of HfO_2. Weak activity observed in the forbidden ν_3 mode for TiO_2 and ZrO_2 is attributed to Herzberg–Teller coupling to the $\tilde{A}^2B_2$ excited state.

I. Introduction

The Group 4 transition metal oxides are an important class of materials, with extensive applications as catalysts, catalyst supports, photocatalysts, dielectric materials, and corrosion resistant materials.[1] Of these, TiO_2 is the most extensively-studied, both theoretically and experimentally.[2] It has tremendous industrial importance as a white pigment, and a considerable line of research is dedicated to the photochemistry of TiO_2 for possible applications in catalysis and organic material degradation.[2–5] It is also a key material in dye-sensitized solar cells.[6] ZrO_2 is primarily used in refractory ceramics due to its high melting temperature and chemical stability.[7] HfO_2, with its high dielectric constant, is used as a gate insulator material for field-effect transistors.[8–10] The study of these materials under controllable conditions, however, has been hampered by experimental difficulties. Even basic values like the work function are difficult to obtain with great precision; surface-sensitive measurements are extremely susceptible to point defects and trace adsorbates.[1,2,11,12]

Clusters of the metal oxides are also of interest in their own right.[13–18] Size-specific clusters have been suggested as a model for surface defect sites, which may have qualitatively different reactivities compared to the ideal surface.[19] Small clusters in particular are amenable to spectroscopy, reactivity studies, and theory, and serve as a way to follow the changes resulting as a function of size. One can also gain insight into reactions that occur on metal and metal oxide surfaces through gas phase chemistry involving size-selected clusters whose chemical composition is similar to that of a catalyst.[13,20] Much of the work in this area has focused on mass spectrometry, but more recently, spectroscopic tools have been developed to characterize the structure of the clusters themselves[21,22] and, to a lesser extent, the intermediates formed when chemical reactions are catalyzed by a small cluster.[23] In our laboratory, we have developed a high resolution negative ion photodetachment technique, slow electron velocity-map imaging (SEVI),[24] and have combined it with ion trapping and cooling,[25] resulting in an instrument that is particularly well-suited to spectroscopic studies of metal oxide clusters. In this article, we focus on spectroscopy of the smallest subunit of the Group 4 dioxides, the triatomic MO_2 species, by SEVI of cold MO_2^- anions.

A considerable amount of spectroscopic work has been carried out on the MO_2 species. Electrostatic deflection experiments established that TiO_2 and ZrO_2 have a permanent dipole moment, and therefore do not have a $D_{\infty h}$ dioxo structure.[26] IR spectra have been recorded for MO_2 isolated in an inert gas matrix;[27] emission spectra of matrix-isolated TiO_2 have also been observed.[28] TiO_2 was the first polyatomic transition metal oxide studied in the gas phase by emission and infrared absorption spectroscopy, though high temperatures and low resolution complicated the analysis.[29,30] Anion photoelectron (PE) spectra of TiO_2^-, ZrO_2^-, and HfO_2^- have been reported,[31–33] all of which have exhibited partially-resolved vibrational structure. The rotational spectra of all three neutral species have been measured by Fourier-transform microwave (FTMW) spectroscopy, giving accurate and precise values for the vibrational ground state M=O bond lengths and OMO bond angles.[34–37]

[a] *Department of Chemistry, University of California, Berkeley, California 94720, USA*
[b] *Chemical Sciences Division, Lawrence Berkeley National Laboratory, Berkeley, California 94720, USA. E-mail: dneumark@berkeley.edu*

For TiO_2 and ZrO_2, the first excited singlet state has also been studied by laser-induced fluorescence (LIF) with optical Stark effects, resonant multi-photon ionization (REMPI), and dispersed fluorescence (DF), revealing term energies, vibrational frequencies, and dipole moments.[38–40] High-resolution photoionization spectroscopy has also been used to study the TiO_2^+ cation.[41]

As is the case with cluster systems, many theoretical studies focus on the structural evolution of the M_xO_y clusters as a function of size and composition.[42–49] Even more studies have calculated various properties of the triatomic MO_2, the monomeric subunit of the stoichiometric $(MO_2)_n$ clusters. For the triatomic TiO_2, ground state properties have been determined by Hartree–Fock,[27,42] many different density functional theory approaches (DFT),[43,44,48,50–53] multireference configuration interaction (MRCI),[53] and coupled-cluster theory.[48,51] Excited state energies have been calculated by time-dependent DFT (TDDFT)[54] and MRCI.[53] Much less work has been done on the zirconium and hafnium dioxide monomers. They have been studied with HF,[27] DFT,[32,49,55] and CCSD(T).[32,49,56,57] All calculations support the dioxo C_{2v} bent structures for the anion and neutral MO_2 species.

In this work, we report high-resolution anion photoelectron spectra of the Group 4 metal dioxide monomers using slow electron velocity-map imaging (SEVI).[24] This method typically yields photoelectron spectra with sub-meV resolution. It is particularly powerful when combined with cryogenic ion cooling, which quenches any hot bands, reduces spectral congestion, and thus simplifies analysis of the resulting spectra. Here, we obtain vibrationally-resolved spectra of transitions to the ground state MO_2 species with considerably higher resolution ($<$1 meV) than previous PE spectra (25–35 meV) and DF studies ($<$10 meV), giving more accurate values of electron affinities and new values for vibrational frequencies. For modeling our spectra using Franck–Condon simulations, we use the neutral geometries as a reference to obtain the anion MO_2^- geometries.

II. Experimental

The experimental apparatus has been described in detail previously.[24,25,58] Anions of interest are formed and then cooled to their ground vibrational state in a cryogenic RF ion trap. They are then mass-selected and photodetached and the electron kinetic energies (eKE) are measured using a velocity-map imaging (VMI)[59] spectrometer, optimized to measure low-eKE electrons. The electron binding energies (eBE) are given by energy conservation, eBE = $h\nu$ − eKE.

Metal oxide ions were produced by a laser ablation source with a solid disc target, based on a design developed by the Smalley group.[60] At a 20 Hz repetition rate, a 2–10 mJ pulse of 532 nm radiation from a Q-switched Nd:YAG laser was focused onto the surface of a titanium, zirconium, or hafnium disc. To prevent uneven target surface damage and thus an unstable ion signal, the target discs were translated and rotated so that the entire surface was evenly worn down. The resulting plasma was quenched and entrained by a burst of helium buffer gas from an Even–Lavie valve.[61] There was sufficient residual oxygen in the buffer gas for production of the desired oxide ions. The ions were guided to an RF ion trap held at 5 K by a closed-cycle refrigerator. While stored in the ion trap, they were thermalized using a cryogenic mix of 20 : 80 H_2 : He buffer gas for 40 ms. Under identical ion production and cooling conditions, we have measured an ion temperature of 10 K for C_5^-.[25]

After the ions were cooled, they were mass-selected in a time-of-flight mass spectrometer. The ions selected were the most abundant isotopologue of each MO_2^- species, $^{48}Ti^{16}O_2^-$, $^{90}Zr^{16}O_2^-$, and $^{180}Hf^{16}O_2^-$. Upon reaching the interaction region of the VMI spectrometer, the ion packets were photodetached by the output of a Nd:YAG-pumped tunable dye laser (Radiant Dyes NarrowScan). The photoelectrons were projected onto an imaging detector by the VMI electrostatic lens.[59,62] The laser polarization defined the axis of cylindrical symmetry, and the radial and angular distributions were reconstructed using the inverse-Abel algorithm of Hansen and Law.[63]

The VMI spectrometer was calibrated for the well-established detachment transitions of O^- and S^-.[64] The VMI resolving power, eKE/ΔeKE, where ΔeKE is the energy resolution, is approximately a constant function of eKE, resulting in high resolution at low eKE. SEVI uses low extraction potentials on the VMI electrodes, allowing for an expanded view of the high-resolution/low-eKE portion of the photoelectron spectra. Typical peak widths with atomic systems are 5.3 cm^{-1} FWHM at 50 cm^{-1} above threshold; at only 13 cm^{-1} above threshold, peak widths narrow to 2.6 cm^{-1}. For the triatomic metal dioxide systems in this report, typical peak widths were 10 cm^{-1} FWHM at 20 cm^{-1} above threshold. Unresolved rotational transitions account for the additional line broadening compared to other species studied using this instrument, all of which had smaller rotational constants.[65–67] As the resolution is highest at low eKE, the laser frequency was tuned to obtain a series of high-resolution spectra over a limited eKE range. Individual scans were spliced together to form composite spectra of the entire band; the intensity of each splice was scaled to the appropriate low-resolution overview spectrum.

The photoelectron angular distribution (PAD) is also measured by VMI. For one-photon detachment, the PAD is given by the expression[68,69]

$$I(\theta) = \frac{\sigma}{4\pi}(1 + \beta P_2(\cos(\theta))) \quad (1)$$

where θ is the angle relative to laser polarization and P_2 is the second-order Legendre polynomial. β is the term defining the angular distribution and lies between values of 2 and −1, corresponding to the limits of a PAD parallel to and perpendicular to the polarization axis. As β is dependent on eKE, we cannot assign a single value for β for a given transition.[68,70,71] However, it is typically only positive or negative-to-zero for a particular transition,[70] so peaks with $\beta > 0.1$ are labeled with a "+" PAD while those with $\beta < 0.1$ are given a "−" PAD.

III. Calculations

The Group 4 MO_2 species are well-established as C_{2v} bent metal-oxo species with structures as shown in Fig. 1. The metal and

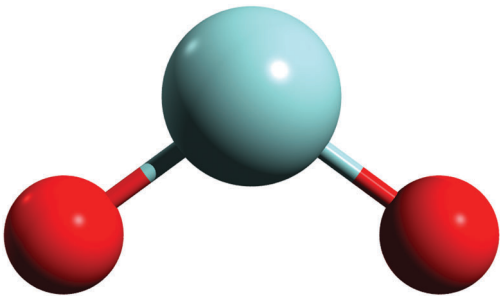

Fig. 1 C_{2v} dioxo structure of the Group 4 triatomic metal dioxides.

two oxygen atoms form two σ and two π bonds, for a nominal bond order of two, a d^0 configuration, and a closed-shell $^1A_1$ electronic state in the neutral species. The excess electron in the anion fills into an empty metal s + d orbital, forming a $^2A_1$ state.

Previous studies by Li and Dixon have found that the BP86 density functional describes the metal dioxide structures and energetics reasonably well compared to high-level *ab initio* theory and experimental results.[48,49] Since the BP86 functional has a known acceptable performance for these systems, we use it to calculate the anion and neutral energies, geometries, and harmonic vibrational frequencies. For the metal atoms, the triple-zeta LANL2TZ basis set was used along with the Hay and Wadt effective core potentials to partially account for relativistic effects.[72,73] The Pople-style 6-311+G* basis set was used for the oxygen atoms. Electronic structure calculations, geometry optimizations, and vibrational analyses were performed using the Gaussian 09 program.[74]

Franck–Condon (FC) simulations of the spectra were calculated using the ezSpectrum program,[75] which calculates FC intensities in the harmonic approximation but with full Duschinsky mixing of the normal modes.[76] As threshold effects may influence relative peak intensities at low eKE,[77] the FC simulations are compared to the low-resolution, high-eKE overview spectra. The stick spectra are convolved using a Gaussian with a relative energy resolution of 3%, the instrumental resolution at high eKE.

IV. Results

Photoelectron spectra of the MO_2^- anions are shown in Fig. 2–4 for M = Ti, Zr, and Hf, respectively. A lower-resolution overview spectrum is displayed on top (blue), taken at photon energies of 15 797 cm^{-1} for Ti and Zr, and 19 991 cm^{-1} for Hf. High-resolution SEVI spectra are spliced together underneath (black), chosen to maximize resolution for the transitions of interest. Insets in Fig. 2 and 3 show the region around peak B in the TiO_2^- and ZrO_2^- spectra. Our dye laser cannot output solely tunable radiation near 18 000 cm^{-1}, as in that region the oscillator can parasitically lase from the second-order Littrow configuration of the grating, superimposing fixed wavelength light on top of the desired tunable light. Consequently, high-resolution spectra are not taken for the features near 18 000 cm^{-1} in HfO_2^-.

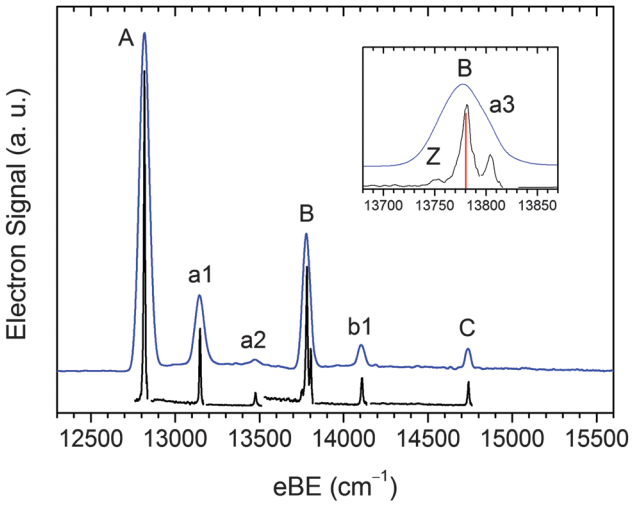

Fig. 2 SEVI spectra of TiO_2^-. The top trace (blue) is a low-resolution overview scan, while the bottom traces (black) are segments of high-resolution scans. An inset expands the congested area around peak B, with FC simulations shown as the stick spectrum (red).

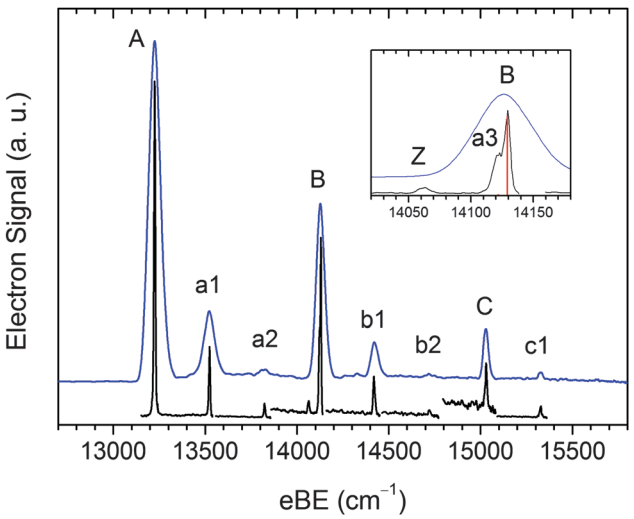

Fig. 3 SEVI spectra of ZrO_2^-. The top trace (blue) is a low-resolution overview scan, while the bottom traces (black) are segments of high-resolution scans. An inset expands the congested area around peak B, with FC simulations shown as the stick spectrum (red).

Each spectrum comprises a band that covers ~2500 cm^{-1} and shifts to increasingly higher eBE as the metal becomes heavier, although the shift is much larger between Zr and Hf than between Ti and Zr. The largest peak in the SEVI spectra of all three species is at lowest eBE and is assigned as the vibrational origin. The spectra exhibit two clear vibrational progressions, with frequencies around 900–1000 cm^{-1} and 300 cm^{-1}. The peaks are labeled to highlight this consistency between all three species; peaks A–C are spaced at 900–1000 cm^{-1}, while a1–a3, b1–b2, *etc.* are offset in multiples of ~300 cm^{-1} from A, B, *etc.* This relatively simple pattern of peaks is characteristic of photodetachment to a single neutral electronic state with only two Franck–Condon active modes. Peak Z in the TiO_2^- and

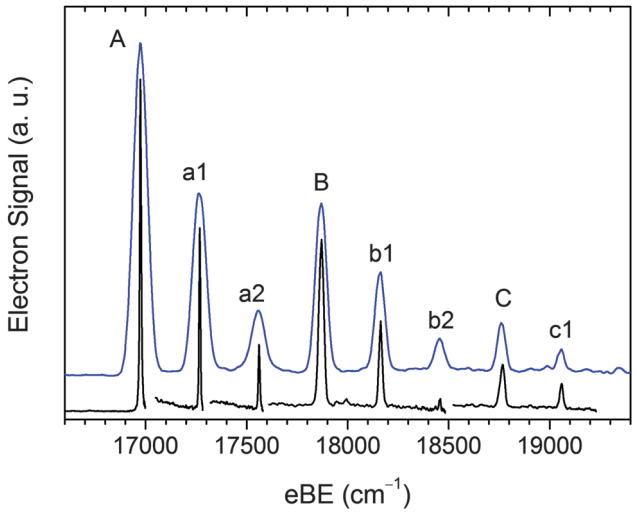

Fig. 4 SEVI spectra of HfO_2^-. The top trace (blue) is a low-resolution overview scan, while the bottom traces (black) are segments of high-resolution scans.

ZrO_2^- spectra (see insets) does not correspond to either of the two progressions. Peak Z also has a PAD with negative β, while all other observed transitions have a positive β.

Peak positions and assignments (see below) are summarized in Tables 1–3 for the respective metal oxides. Calculated geometries, frequencies, and zero-point vibrational energy corrected electron affinities (EAs) for all three species are reported in Table 4. The experimentally determined values from this work and previous studies are summarized in Table 5. Due to broadening from unresolved rotational structure, peak position errors are reported as $\pm\sigma$ of a Gaussian peak fit, 4–6 cm^{-1} in this report.

Table 1 Peak positions (cm^{-1}), shifts from the origin (cm^{-1}), PADs, and vibrational assignments for the TiO_2^- spectra

Peak	Position	Shift	PAD	Assn.
A	12 818	0	+	0_0^0
a1	13 147	330	+	2_0^1
a2	13 476	659	+	2_0^2
Z	13 752	935	−	3_0^1
B	13 781	963	+	1_0^1
a3	13 804	986	+	2_0^3
b1	14 109	1292	+	$1_0^1 2_0^1$
C	14 740	1923	+	1_0^2

Table 2 Peak positions (cm^{-1}), shifts from the origin (cm^{-1}), PADs, and vibrational assignments for the ZrO_2^- spectra

Peak	Position	Shift	PAD	Assn.
A	13 225	0	+	0_0^0
a1	13 523	298	+	2_0^1
a2	13 823	598	+	2_0^2
Z	14 062	837	−	3_0^1
a3	14 121	896	+	2_0^3
B	14 129	905	+	1_0^1
b1	14 420	1196	+	$1_0^1 2_0^1$
b2	14 722	1497	+	$1_0^1 2_0^1$
C	15 031	1806	+	1_0^2
c1	15 327	2102	+	$1_0^2 2_0^1$

Table 3 Peak positions (cm^{-1}), shifts from the origin (cm^{-1}), PADs, and vibrational assignments for the HfO_2^- spectra

Peak	Position	Shift	PAD	Assn.
A	16 974	0	+	0_0^0
a1	17 268	293	+	2_0^1
a2	17 561	587	+	2_0^2
B	17 869	895	+	1_0^1
b1	18 164	1189	+	$1_0^1 2_0^1$
b2	18 457	1483	+	$1_0^1 2_0^2$
C	18 766	1792	+	1_0^2
c1	19 058	2084	+	$1_0^2 2_0^1$

Table 4 Calculated EAs (eV), bond lengths (Å), bond angles (degrees), and vibrational frequencies (cm^{-1}) for the MO_2 species

	TiO_2^-	TiO_2	ZrO_2^-	ZrO_2	HfO_2^-	HfO_2
EA		1.70		1.78		2.23
R	1.695	1.661	1.842	1.803	1.823	1.784
θ	112.0	110.5	108.2	106.2	109.7	105.7
ν_1	912	977	820	878	817	870
ν_2	313	337	274	299	262	300
ν_3	890	952	763	822	740	791

V. Discussion

a. Assignments

In agreement with previous experimental and theoretical work, the single electronic band for each species in the SEVI spectra corresponds to the $\tilde{X}^1A_1 \leftarrow \tilde{X}^2A_1$ transition, with electron detachment from the anion a_1 SOMO.[31–33,48,49,51,56,57] The calculated EAs are also in good agreement with the vibrational origins of the corresponding bands, with calculated EAs consistently overestimated by 0.1 eV, a reasonable error with DFT.[78]

The PADs, which have not been measured before, also support this assignment. In the qualitative model developed by Surber *et al.*[79] for photodetachment of an anion with C_{2v} symmetry, a positive β can only result by electron detachment from an orbital of the a_1 irreducible representation. Almost all of the peaks have a PAD with a positive β, consistent with the assigned transition.

Upon photodetachment, the metal dioxides are calculated to have bond length decreases of 0.34–0.39 Å and bond angle decreases of 1.5–4.0°. Therefore, we expect progressions in both the ν_1 symmetric stretch and ν_2 bend modes of the neutral MO_2 species, and, as noted above, two progressions are indeed apparent in the anion SEVI spectra. The main progression is that of peak A–C, with a spacing of 962 cm^{-1} for TiO_2, 904 cm^{-1} for ZrO_2, and 896 cm^{-1} for HfO_2. These values match within 30 cm^{-1} of the corresponding calculated ν_1 frequencies in Table 4. Owing to ion cooling, there are no peaks visible below peak A, the vibrational origin. Peaks B and C, then, correspond to the 1_0^1 and 1_0^2 transitions.

Peaks A, a1, and a2 form a clear progression with only at most a 2 cm^{-1} difference between the intervals A–a1 and a1–a2.

Table 5 Experimental values from previous studies and this work for the EAs (eV), bond lengths (Å), bond angles (degrees), and vibrational frequencies (cm^{-1}) for the MO_2 species

	TiO_2^-	TiO_2	ZrO_2^-	ZrO_2	HfO_2^-	HfO_2
Previous results						
EA		1.59(3)[a]		1.64(3)[b]		2.14(3)[b], 2.125(10)[c]
R		1.651[d]		1.7710(7)[e]		1.7764(4)[f]
θ	128(5)[g]	111.57[d], 113(5)[g]	128(4)[g]	108.11(8)[e], 113(5)[g]	132(4)[g]	107.51(1)[f], 115(5)[g]
ν_1		960(40)[a], 978(7)[h], 946.9[g]		887(40)[b], 898(1)[i], 884.3[g]		887(40)[b], 890(30)[c], 883.4[g]
ν_2		323(1)[h]		287(2)[i]		290(30)[c]
ν_3	878.4[g]	917.7[g]	761.4[g]	808(3)[i], 818[g]	747.9[g]	814[g]
This work						
EA		1.5892(5)		1.6397(5)		2.1045(5)
R	1.682(4)[j]		1.803(4)[j]		1.811(4)[j]	
θ	113.6(4)[j]		110.3(4)[j]		111.5(4)[j]	
ν_1		962(3)		904(3)		896(7)
ν_2		329(3)		299(2)		293(3)
ν_3		935(6)		837(5)		

[a] PES, ref. 31. [b] PES, ref. 32. [c] PES, ref. 33. [d] FTMW, ref. 34. [e] FTMW, ref. 36. [f] FTMW, ref. 37. [g] Matrix isolation FTIR, ref. 27. [h] DF, ref. 39. [i] DF, ref. 40. [j] Values obtained relative to the neutral FTMW results.

By comparison with the calculated vibrational frequencies, there is no doubt that these constitute the 2_0^n (n = 0–2) progression for each species. The next member of the sequence lies among the cluster of peaks Z, B, and a3 in the TiO_2 and ZrO_2 spectra. An analogous cluster may be present in HfO_2. However, as mentioned in Section IV, high-resolution scans were not obtained near peak B. By extrapolation of the sequence, the 2_0^3 transition is assigned to the a3 peaks; their positions agree with the extrapolated values to less than 2 cm^{-1} as well, while the neighboring peak B would be off by 9 or 25 cm^{-1} and peak Z further still. Furthermore, peak B is the most intense peak of the cluster and is already assigned to the 1_0^1 transition. The splittings between the 1_0^1 and 2_0^3 transitions are resolved by SEVI, even for ZrO_2, where peak a3 is a shoulder of peak B with only a difference of 9 cm^{-1} between the two peak centers.

Peaks b1 and b2 are assigned as the $1_0^1 2_0^1$ and $1_0^1 2_0^2$ transitions based on their offset from B compared to those of a1 and a2 relative to A. Continuing the trend of peaks A–B, the C peaks are the 1_0^2 transitions, and the c1 peaks are the $1_0^2 2_0^1$ transitions. The fit of all the assigned peaks to an uncoupled harmonic oscillator model has deviations of less than 4 cm^{-1}. We obtain ν_1 and ν_2 vibrational frequencies for all three MO_2 neutral species, as summarized in Table 5. As peak A is assigned the vibrational origin in all three spectra, we obtain EAs of 1.5892(5) eV for TiO_2, 1.6397(5) eV for ZrO_2, and 2.1045(5) eV for HfO_2.

b. Vibronic coupling

Although nearly all features in the MO_2^- SEVI spectra can be satisfactorily assigned, the presence of peak Z in the high resolution scans of TiO_2 and ZrO_2 is anomalous. All combinations of the totally symmetric ν_1 and ν_2 modes are accounted for. In the FC approximation, only Δv = even transitions are allowed for the non-totally symmetric ν_3 mode. As the anion is in its ground vibrational state, the lowest such transition would be the 3_0^2 peak. However, this transition is calculated at 1500–1900 cm^{-1} above the origin, twice the value of peak Z relative to the origin. Prior experimental and theoretical work has also ruled out the existence of an excited electronic state so close to the ground state.[31,53,54] The most reasonable explanation is that peak Z is a forbidden $\Delta v_3 = 1$ excitation.

Such features are often seen in SEVI and PE spectra[80–85] and can be allowed by the Herzberg–Teller coupling of two electronic states el′ and el″

$$\Gamma_{el'} \otimes \Gamma_{\nu} \otimes \Gamma_{el''} \supset \Gamma_{A} \quad (2)$$

If the product of the irreducible representations of the two states and the coupling mode ν contain the totally symmetric representation A, then odd quanta excitation of that mode could be allowed. Using the Mulliken convention for C_{2v} systems,[86] the ν_3 mode has b_2 symmetry and the ground neutral state is A_1. Thus, the 3_0^1 transition could be allowed through vibronic coupling to an excited B_2 state. In fact, the lowest-lying singlet excited state for all three neutral species is the $\tilde{A}^1B_2$ state, with experimental term energies of 2.1813(6) eV, 2.0218(10) eV, and 1.3(1) eV for TiO_2, ZrO_2, and HfO_2, respectively.[33,39,40]

The PAD of peak Z also supports this interpretation. All other peaks have a positive β, in agreement with a $\tilde{X}^1A_1 \leftarrow \tilde{X}^2A_1$ electronic transition. If peak Z is borrowing intensity from the $\tilde{A}^1B_2$ state, it should also be borrowing electronic state character and hence should have a PAD resembling that of $\tilde{A}^1B_2 \leftarrow \tilde{X}^2A_1$. That transition undergoes electron detachment from a b_2 orbital, and based on the model by Surber *et al.* should have a negative-to-zero β for the PAD.[79] Although the signal is weak for peak Z, it is sufficient to determine that the β does not go above 0.1, consistent with the picture of intensity-borrowing from the $\tilde{A}^1B_2 \leftarrow \tilde{X}^2A_1$ transition.

c. Franck–Condon simulations

In order to extract information on the geometry changes that occur upon photodetachment, we can compare our experimental spectra to FC simulations. Owing to the Wigner threshold law,[77] the relative intensity of transitions in the high-resolution, low-eKE scans may not accurately represent the true intensities. Hence, we compare the FC simulations with the low-resolution

overview scans. The top trace in each panel of Fig. 5 shows the overview spectrum for each species (blue), the FC simulation just below (red) with the origin shifted to match experiment, and the FC simulation at the bottom (black) with optimized geometry changes and vibrational frequencies. By only adjusting the position of the vibrational origin, the FC simulations already qualitatively match the experiment, further confirming the assigned detachment transitions. However, the FC simulations of all species overestimate the intensity of the 1_0^n progression, suggesting that the calculated geometries overestimate the bond length changes upon electron detachment.

The geometry changes can be deduced by adjusting the FC simulation parameters to fit our experimental spectra. As the neutral vibrational ground state geometries have been measured to high precision by FTMW spectroscopy,[34–37] the corresponding anion geometries can be extracted. The FC simulations depend on the anion and neutral geometries, normal mode coordinates, and vibrational frequencies. The neutral vibrational frequencies are set to the experimentally determined values for a better agreement with simulation. We fix the neutral geometries to the values from FTMW spectroscopy and adjust the anion bond angles and bond lengths for a best fit of the FC simulations to the overview spectra, assuming that these small changes affect only the displacement of the normal coordinates between the anion and neutral species. We obtain M=O bond lengths and OMO bond angles for all three metal dioxide anions, summarized in Table 5. Errors reported are those given by the displacement in geometry that would give a 20% error in the intensity of the 1_0^1 or 2_0^1 transitions. The only prior experimental measurement for the anion geometries was an estimate of bond angles by the isotope shifts for the ν_3 mode in an inert argon matrix,[27] yielding bond angles of 128(5)°, 128(4)°, and 132(4)° for TiO_2^-, ZrO_2^-, and HfO_2^-. These values are higher than what we deduce by 15–20°. However, bond angles for the neutral dioxides were obtained by the same method and were found to be higher by 5–10° compared to the accurate values obtained by FTMW, suggesting a systematic overestimation of bond angles in that work.

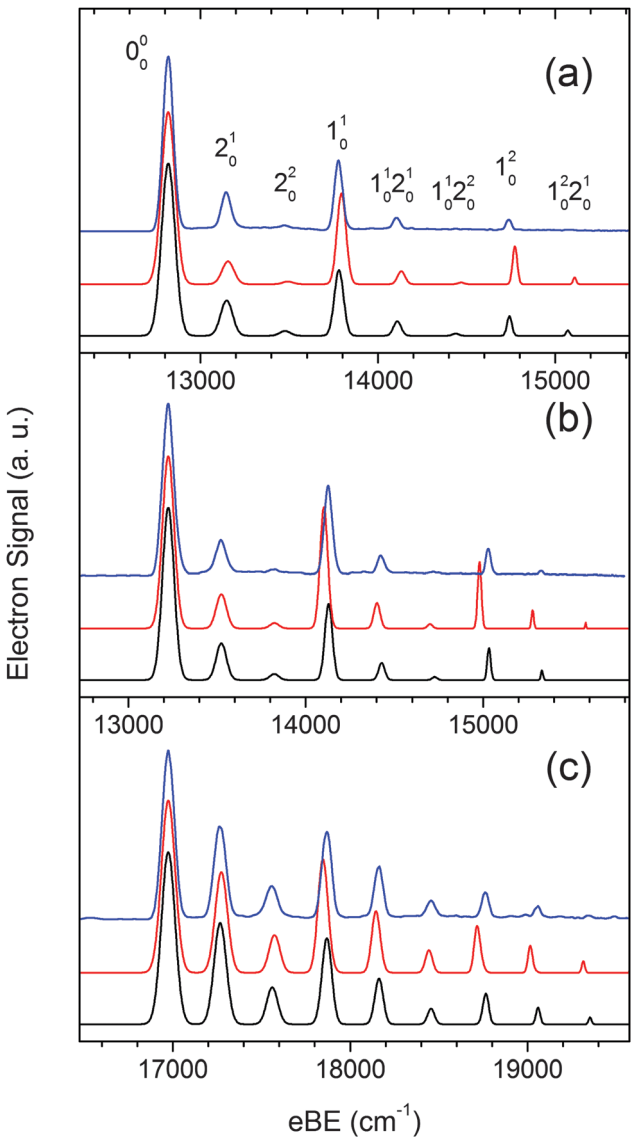

Fig. 5 FC fits to the overview spectra of TiO_2 (a), ZrO_2 (b), and HfO_2 (c). The top traces (blue) are the overview spectra from Fig. 2–4. The middle traces (red) are the FC simulations at the BP86/LANL2TZ geometries. Anion geometries and neutral vibrational frequencies are adjusted so the bottom traces (black) are fit to the overview spectra.

While the relative intensities of peaks in the overview spectra match the FC simulations, those of high-resolution scans do not, as shown in the insets of Fig. 2 and 3. In the calculated FC progressions shown as red stick spectra, the 2_0^3 transition (peak a3) has negligible intensity relative to 1_0^1 (peak B) for the TiO_2 and ZrO_2 spectra. However, the high-resolution scans highlighting those two peaks show the 2_0^3 transition to be almost half as intense as 1_0^1. The 2_0^3 transition may borrow intensity from the nearby 1_0^1 transition through Fermi resonance effects. There may also be threshold effects influencing relative peak heights, as those transitions are only resolved in the low-eKE scans.

d. Comparison to previous work

The EAs obtained here are a significant improvement over those from previous PE experiments. As summarized in Table 5, our EAs for TiO_2 and ZrO_2 are more precise by two orders of magnitude and are well within the reported error bounds of prior work. However, while our EA for HfO_2 is within 6% of previous values, it lies outside the error bounds of those measurements. We find an EA of 2.1045(5) eV, lower than the values of 2.13(3) eV[32] and 2.125(10) eV[33] obtained by anion PES with a time-of-flight electron spectrometer. Surprisingly, both prior experiments obtained EAs consistent with each other and inconsistent with ours. However, the earlier PE spectra of HfO_2^- showed more intensity from hot bands than the other MO_2^- spectra obtained on the same instruments, possibly complicating the accurate establishment of the vibrational origin. In particular, the unresolved 2_n^n sequence bands could result in a shift of the center-of-mass of the origin to higher eBE. While the 2_1^1 transition is only predicted at 38 cm^{-1} above the origin, uncertainties in calculated frequencies could well mean that the shift is larger.

The SEVI spectra also yield accurate vibrational frequencies for the FC active modes, ν_1 and ν_2. Owing to vibronic coupling, the ν_3 mode is also weakly observed in the titanium and zirconium species. Matrix isolation techniques have been the most accessible method of obtaining experimental vibrational information of isolated metal oxide systems.[14] The Group 4 MO_2 systems have been studied by FTIR spectroscopy while frozen in an argon matrix.[27] All three modes are symmetry-allowed in IR spectroscopy, but the calculated IR intensities go as $\nu_3 > \nu_1 > \nu_2$, and in that work vibrational frequencies were only assigned for the ν_1 and ν_3 modes. Those values differ from our value by less than 20 cm^{-1}, an acceptable deviation for values obtained in a perturbative matrix. Previous anion PES experiments have yielded ν_1 frequencies for all three species, as well as the ν_2 frequency for HfO_2. Our values are consistent with those results and well within the error bounds as given in Table 5.

The vibrational frequencies for TiO_2 and ZrO_2 have also been obtained by Steimle and co-workers *via* gas phase dispersed fluorescence (DF), with the values summarized in Table 5.[38–40] While the vibrational frequencies assigned by DF and SEVI are close to each other, the differences are significant based on the reported error bounds of each experiment.

Both experiments obtained frequencies by assigning the vibrational structure of electronic transitions. The DF experiments recorded several different emission spectra from excitation to various vibrational states of the $\tilde{A}^2B_2$ electronic state, while the SEVI spectra are from direct one-photon detachment. Consequently, the DF frequency assignments made use of many more observed vibronic transitions than the SEVI assignments. For example, the DF assignments of ZrO_2 used 268 peaks, compared to 10 for SEVI. However, the spectral resolution is higher for the SEVI experiment. While our peak FWHM was limited to 10 cm^{-1} due to the unresolved rotational structure, the DF spectrometer had a spectral FWHM of $\sim$20 Å, corresponding to $\sim$50 cm^{-1} in the region of fluorescence. Moreover, the SEVI spectra match the FC simulations well, while the DF spectra are not modeled, leaving it unclear how well the DF assignments match with calculated peak intensities. In light of the higher resolution of our spectra, combined with their simplicity and our ability to model the intensities easily, our vibrational frequencies for the TiO_2 and ZrO_2 neutral ground states should be more accurate than those obtained by DF.

While the MO_2 species discussed here have been studied by many different techniques, considerably less is known about the gas phase spectroscopy of metal oxide clusters with multiple metal centers. IR photodissociation (IRPD) spectroscopy has had the most success in obtaining vibrational and geometric structure of clusters,[18] especially with the addition of cryogenic ion cooling.[87] Anion PES has been useful for providing electronic energetics, but lower resolution and spectral congestion from hot bands have limited vibrational information.[15,17,88] SEVI with cryogenic ion cooling can resolve both these problems, allowing for the acquisition of PE spectra with resolution comparable to IRPD spectroscopy. Moreover, vibrational and electronic spectroscopy selection rules are often complementary, and vibrationally-resolved PE spectra can be compared with IR spectra to check the validity of both. SEVI thus has the potential for obtaining vibrationally-resolved spectra of more complicated polymetal species, and this potential will be exploited by our laboratory in the very near future.

VI. Conclusions

High-resolution photoelectron spectra are reported for the Group 4 metal dioxide anions, TiO_2^-, ZrO_2^-, and HfO_2^-. Improved electron affinities are reported for all three neutral species with sub-meV resolution. In addition, most vibrational frequencies of the neutral species are reported with higher precision than previous studies. By fitting the simulated spectrum to the experiment, the anion geometries are also determined. The combination of ion cooling with a high-resolution spectrometer allows for straightforward analysis of photoelectron spectra.

Acknowledgements

This research is funded by the Air Force Office of Scientific Research under Grant No. FA9550-12-1-0160 and the Defense University Research Instrumentation Program under Grant No. FA9550-11-1-0300. M.L.W. thanks the National Science Foundation for a graduate research fellowship.

References

1 V. E. Henrich and P. A. Cox, *The Surface Science of Metal Oxides*, University Press, Cambridge, 1994.
2 U. Diebold, *Surf. Sci. Rep.*, 2003, **48**, 53.
3 A. Fujishima and K. Honda, *Nature*, 1972, **238**, 37.
4 O. Carp, C. L. Huisman and A. Reller, *Prog. Solid State Chem.*, 2004, **32**, 33.
5 A. Fujishima, X. Zhang and D. A. Tryk, *Surf. Sci. Rep.*, 2008, **63**, 515.
6 M. Grätzel, *Acc. Chem. Res.*, 2009, **42**, 1788.
7 N. N. Greenwood and A. Earnshaw, *Chemistry of the Elements*, Elsevier, 1998.
8 G. D. Wilk, R. M. Wallace and J. M. Anthony, *J. Appl. Phys.*, 2001, **89**, 5243.
9 R. Chau, S. Datta, M. Doczy, B. Doyle, J. Kavalieros and M. Metz, *IEEE Electron Device Lett.*, 2004, **25**, 408.
10 R. John, *Rep. Prog. Phys.*, 2006, **69**, 327.
11 K. Onda, B. Li and H. Petek, *Phys. Rev. B: Condens. Matter Mater. Phys.*, 2004, **70**, 045415.
12 A. Borodin and M. Reichling, *Phys. Chem. Chem. Phys.*, 2011, **13**, 15442.
13 D. K. Böhme and H. Schwarz, *Angew. Chem., Int. Ed.*, 2005, **44**, 2336.
14 Y. Gong, M. Zhou and L. Andrews, *Chem. Rev.*, 2009, **109**, 6765.
15 H.-J. Zhai and L.-S. Wang, *Chem. Phys. Lett.*, 2010, **500**, 185.
16 A. W. Castleman, *Catal. Lett.*, 2011, **141**, 1243.
17 J. E. Mann, N. J. Mayhall and C. C. Jarrold, *Chem. Phys. Lett.*, 2012, **525–526**, 1.
18 K. R. Asmis, *Phys. Chem. Chem. Phys.*, 2012, **14**, 9270.

19 K. A. Zemski, D. R. Justes and A. W. Castleman, *J. Phys. Chem. B*, 2002, **106**, 6136.
20 G. E. Johnson, E. C. Tyo and A. W. Castleman, *Proc. Natl. Acad. Sci. U. S. A.*, 2008, **105**, 18108.
21 G. Santambrogio, M. Brummer, L. Woste, J. Dobler, M. Sierka, J. Sauer, G. Meijer and K. R. Asmis, *Phys. Chem. Chem. Phys.*, 2008, **10**, 3992.
22 H. J. Zhai and L. S. Wang, *Chem. Phys. Lett.*, 2010, **500**, 185.
23 A. Fielicke, R. Mitrić, G. Meijer, V. Bonačić-Koutecký and G. von Helden, *J. Am. Chem. Soc.*, 2003, **125**, 15716.
24 D. M. Neumark, *J. Phys. Chem. A*, 2008, **112**, 13287.
25 C. Hock, J. B. Kim, M. L. Weichman, T. I. Yacovitch and D. M. Neumark, *J. Chem. Phys.*, 2012, **137**, 244201.
26 M. Kaufman, J. Muenter and W. Klemperer, *J. Chem. Phys.*, 1967, **47**, 3365.
27 G. V. Chertihin and L. Andrews, *J. Phys. Chem.*, 1995, **99**, 6356.
28 N. S. McIntyre, K. R. Thompson and W. Weltner, *J. Phys. Chem.*, 1971, **75**, 3243.
29 T. C. Devore, *High Temp. Sci.*, 1982, **15**, 219.
30 T. C. Devore and T. N. Gallaher, *High Temp. Sci.*, 1983, **16**, 269.
31 H. Wu and L.-S. Wang, *J. Chem. Phys.*, 1997, **107**, 8221.
32 W. Zheng, K. H. Bowen, J. Li, I. Dąbkowska and M. Gutowski, *J. Phys. Chem. A*, 2005, **109**, 11521.
33 H.-J. Zhai, W.-J. Chen, S.-J. Lin, X. Huang and L.-S. Wang, *J. Phys. Chem. A*, 2012, **117**, 1042.
34 S. Brünken, H. S. P. Müller, K. M. Menten, M. C. McCarthy and P. Thaddeus, *Astrophys. J.*, 2008, **676**, 1367.
35 P. Kania, M. Hermanns, S. Brünken, H. S. P. Müller and T. F. Giesen, *J. Mol. Spectrosc.*, 2011, **268**, 173.
36 D. J. Brugh, R. D. Suenram and W. J. Stevens, *J. Chem. Phys.*, 1999, **111**, 3526.
37 A. Lesarri, R. D. Suenram and D. Brugh, *J. Chem. Phys.*, 2002, **117**, 9651.
38 H. Wang, T. C. Steimle, C. Apetrei and J. P. Maier, *Phys. Chem. Chem. Phys.*, 2009, **11**, 2649.
39 X. Zhuang, A. Le, T. C. Steimle, R. Nagarajan, V. Gupta and J. P. Maier, *Phys. Chem. Chem. Phys.*, 2010, **12**, 15018.
40 A. Le, T. C. Steimle, V. Gupta, C. A. Rice, J. P. Maier, S. H. Lin and C.-K. Lin, *J. Chem. Phys.*, 2011, **135**, 104303.
41 Y.-C. Chang, H. Huang, Z. Luo and C. Y. Ng, *J. Chem. Phys.*, 2013, **138**, 041101.
42 A. Hagfeldt, R. Bergstroem, H. O. G. Siegbahn and S. Lunell, *J. Phys. Chem.*, 1993, **97**, 12725.
43 T. Albaret, F. Finocchi and C. Noguera, *J. Chem. Phys.*, 2000, **113**, 2238.
44 K. S. Jeong, C. Chang, E. Sedlmayr and D. Sülzle, *J. Phys. B: At., Mol. Opt. Phys.*, 2000, **33**, 3417.
45 S. Hamad, C. R. A. Catlow, S. M. Woodley, S. Lago and J. A. Mejías, *J. Phys. Chem. B*, 2005, **109**, 15741.
46 Z.-W. Qu and G.-J. Kroes, *J. Phys. Chem. B*, 2006, **110**, 8998.
47 S. M. Woodley, S. Hamad, J. A. Mejias and C. R. A. Catlow, *J. Mater. Chem.*, 2006, **16**, 1927.
48 S. Li and D. A. Dixon, *J. Phys. Chem. A*, 2008, **112**, 6646.
49 S. G. Li and D. A. Dixon, *J. Phys. Chem. A*, 2010, **114**, 2665.
50 R. Bergström, S. Lunell and L. A. Eriksson, *Int. J. Quantum Chem.*, 1996, **59**, 427.
51 M. B. Walsh, R. A. King and H. F. Schaefer III, *J. Chem. Phys.*, 1999, **110**, 5224.
52 G. L. Gutsev, B. K. Rao and P. Jena, *J. Phys. Chem. A*, 2000, **104**, 11961.
53 F. Grein, *J. Chem. Phys.*, 2007, **126**, 034313.
54 D. J. Taylor and M. J. Paterson, *J. Chem. Phys.*, 2010, **133**, 204302.
55 M. Kaupp, *Chem.–Eur. J.*, 1999, **5**, 3631.
56 D. K. W. Mok, F.-t. Chau, J. M. Dyke and E. P. F. Lee, *Chem. Phys. Lett.*, 2008, **458**, 11.
57 D. K. W. Mok, E. P. F. Lee, F.-t. Chau and J. M. Dyke, *Phys. Chem. Chem. Phys.*, 2008, **10**, 7270.
58 A. Osterwalder, M. J. Nee, J. Zhou and D. M. Neumark, *J. Chem. Phys.*, 2004, **121**, 6317.
59 A. Eppink and D. H. Parker, *Rev. Sci. Instrum.*, 1997, **68**, 3477.
60 S. C. O'Brien, Y. Liu, Q. Zhang, J. R. Heath, F. K. Tittel, R. F. Curl and R. E. Smalley, *J. Chem. Phys.*, 1986, **84**, 4074.
61 U. Even, J. Jortner, D. Noy, N. Lavie and C. Cossart-Magos, *J. Chem. Phys.*, 2000, **112**, 8068.
62 M. B. Doyle, C. Abeyasera and A. G. Suits, NuACQ, http://chem.wayne.edu/suitsgroup/NuACQ.html.
63 E. W. Hansen and P.-L. Law, *J. Opt. Soc. Am. A*, 1985, **2**, 510.
64 C. Blondel, W. Chaibi, C. Delsart, C. Drag, F. Goldfarb and S. Kröger, *Eur. Phys. J. D*, 2005, **33**, 335.
65 J. B. Kim, M. L. Weichman, T. I. Yacovitch, C. Shih and D. M. Neumark, *J. Chem. Phys.*, 2013, **139**, 104301.
66 J. B. Kim, C. Hock, T. I. Yacovitch and D. M. Neumark, *J. Phys. Chem. A*, 2013, **117**, 8126.
67 M. L. Weichman, J. B. Kim and D. M. Neumark, *J. Chem. Phys.*, 2013, **139**, 144314.
68 J. Cooper and R. N. Zare, *J. Chem. Phys.*, 1968, **48**, 942.
69 K. L. Reid, *Annu. Rev. Phys. Chem.*, 2003, **54**, 397.
70 C. Bartels, C. Hock, J. Huwer, R. Kuhnen, J. Schwöbel and B. von Issendorff, *Science*, 2009, **323**, 1323.
71 R. Mabbs, E. R. Grumbling, K. Pichugin and A. Sanov, *Chem. Soc. Rev.*, 2009, **38**, 2169.
72 P. J. Hay and W. R. Wadt, *J. Chem. Phys.*, 1985, **82**, 299.
73 L. E. Roy, P. J. Hay and R. L. Martin, *J. Chem. Theory Comput.*, 2008, **4**, 1029.
74 M. J. Frisch, G. W. Trucks, H. B. Schlegel, G. E. Scuseria, M. A. Robb, J. R. Cheeseman, G. Scalmani, V. Barone, B. Mennucci, G. A. Petersson, H. Nakatsuji, M. Caricato, X. Li, H. P. Hratchian, A. F. Izmaylov, J. Bloino, G. Zheng, J. L. Sonnenberg, M. Hada, M. Ehara, K. Toyota, R. Fukuda, J. Hasegawa, M. Ishida, T. Nakajima, Y. Honda, O. Kitao, H. Nakai, T. Vreven, J. A. Montgomery, J. E. Peralta, F. Ogliaro, M. Bearpark, J. J. Heyd, E. Brothers, K. N. Kudin, V. N. Staroverov, R. Kobayashi, J. Normand, K. Raghavachari, A. Rendell, J. C. Burant, S. S. Iyengar, J. Tomasi, M. Cossi, N. Rega, J. M. Millam, M. Klene, J. E. Knox, J. B. Cross, V. Bakken, C. Adamo, J. Jaramillo, R. Gomperts, R. E. Stratmann, O. Yazyev, A. J. Austin, R. Cammi, C. Pomelli, J. W. Ochterski, R. L. Martin,

K. Morokuma, V. G. Zakrzewski, G. A. Voth, P. Salvador, J. J. Dannenberg, S. Dapprich, A. D. Daniels, Ö. Farkas, J. B. Foresman, J. V. Ortiz, J. Cioslowski and D. J. Fox, *Gaussian 09, Revision C.01*, Gaussian, Inc., Wallingford CT, 2010.
75 V. A. Mozhayskiy and A. I. Krylov, ezSpectrum, http://iopenshell.usc.edu/downloads.
76 F. Duschinsky, *Acta Physicochim. URSS*, 1937, **7**, 551.
77 E. P. Wigner, *Phys. Rev.*, 1948, **73**, 1002.
78 J. C. Rienstra-Kiracofe, G. S. Tschumper, H. F. Schaefer, S. Nandi and G. B. Ellison, *Chem. Rev.*, 2002, **102**, 231.
79 E. Surber, R. Mabbs and A. Sanov, *J. Phys. Chem. A*, 2003, **107**, 8215.
80 K. M. Ervin and W. C. Lineberger, *J. Phys. Chem.*, 1991, **95**, 1167.
81 A. Weaver, D. W. Arnold, S. E. Bradforth and D. M. Neumark, *J. Chem. Phys.*, 1991, **94**, 1740.
82 M. Mayer, L. S. Cederbaum and H. Köppel, *J. Chem. Phys.*, 1994, **100**, 899.
83 K. R. Asmis, T. R. Taylor and D. M. Neumark, *J. Chem. Phys.*, 1999, **111**, 8838.
84 E. Garand, K. Klein, J. F. Stanton, J. Zhou, T. I. Yacovitch and D. M. Neumark, *J. Phys. Chem. A*, 2010, **114**, 1374.
85 K. Klein, E. Garand, T. Ichino, D. Neumark, J. Gauss and J. Stanton, *Theor. Chem. Acc.*, 2011, **129**, 527.
86 R. S. Mulliken, *J. Chem. Phys.*, 1955, **23**, 1997.
87 K. R. Asmis, M. Brummer, C. Kaposta, G. Santambrogio, G. von Helden, G. Meijer, K. Rademann and L. Woste, *Phys. Chem. Chem. Phys.*, 2002, **4**, 1101.
88 L.-S. Wang, in *Photoionization and Photodetachment*, ed. C. Y. Ng, World Scientific, Singapore, 2000, vol. 10, ch. 16.